Supplementary Figures

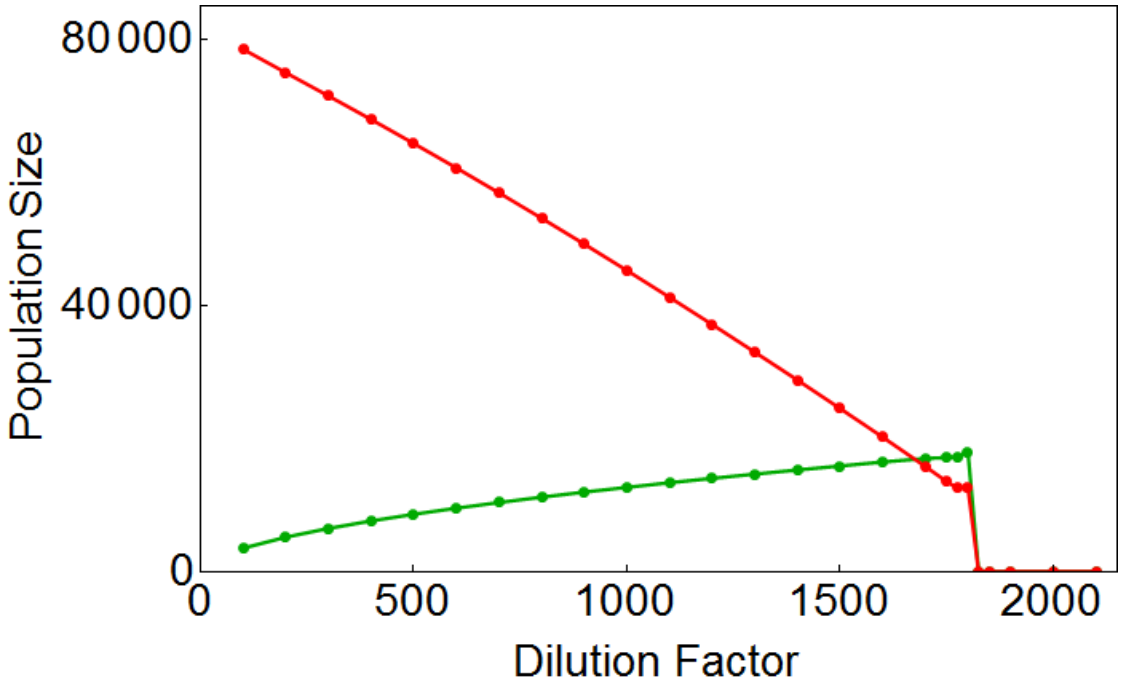

Supplementary Figure 1: Simulation of equilibrium population densities as a function of Dilution Factor has qualitative similarities to experimental results. A noisy, simulated model of our experimental procedure was run at different dilution factors with an array of starting points. The trajectories approached an equilibrium, which was found after letting the simulation run for a prolonged period of time. The ensuing plot shows the simulated equilibrium points for the Producer (green) and Freeloader (red) population densities (in cells/μL). By dilution factors above 1800, all populations go extinct, regardless of the location of the starting points. Due to the Allee effect, which is explicit in the model, the point (0,0) is always a fixed point. Details of the simulation can be found in Supplementary Note 6 and Supplementary Table 1.

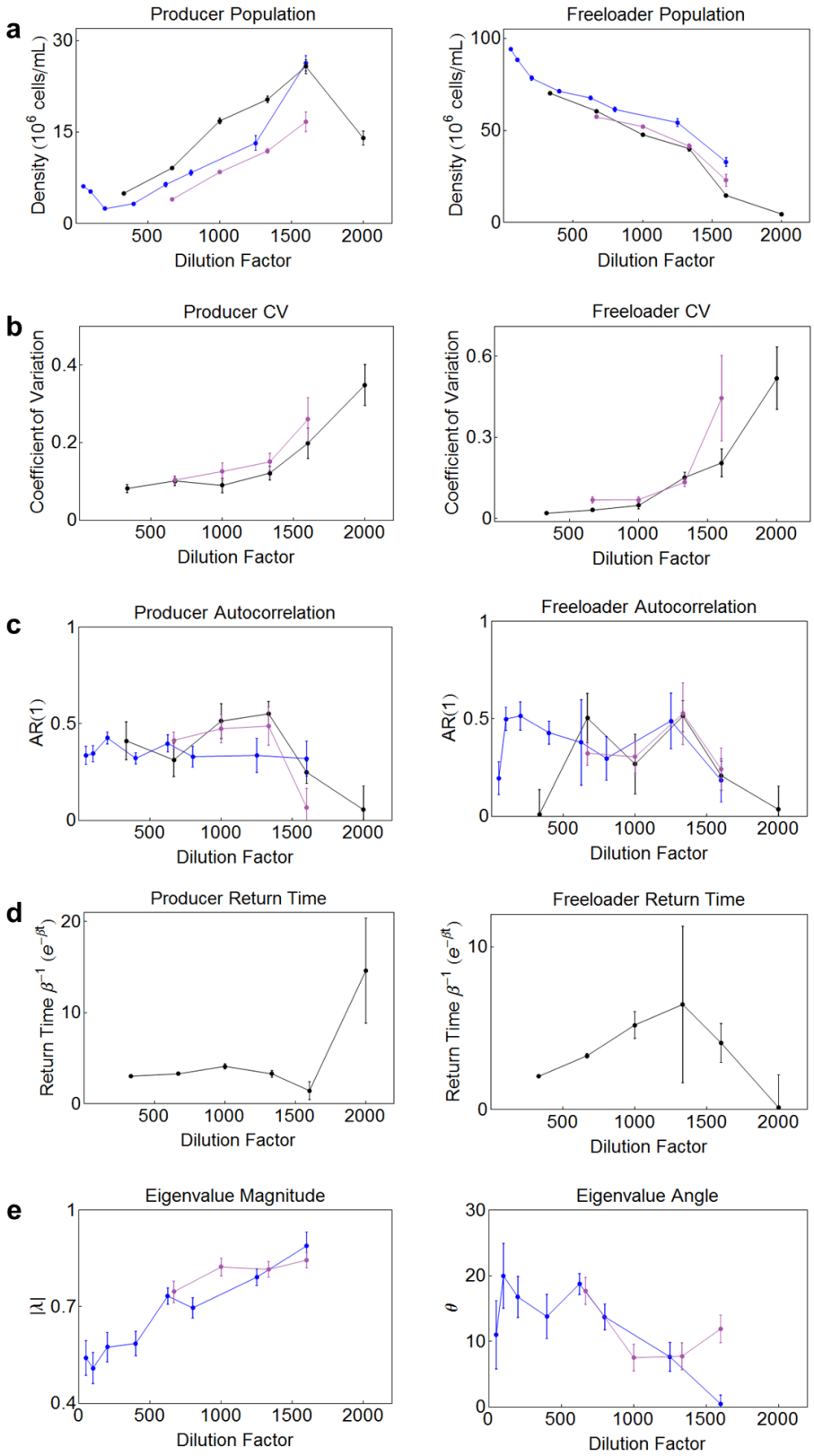
a
Producer Population
Density (10^6 cells/mL)
Dilution Factor
Freeloader Population
Density (10^6 cells/mL)
Dilution Factor
b
Producer CV
Coefficient of Variation
Dilution Factor
Freeloader CV
Coefficient of Variation
Dilution Factor
c
Producer Autocorrelation
AR(1)
Dilution Factor
Freeloader Autocorrelation
AR(1)
Dilution Factor
d
Producer Return Time
Return Time β^{-1} ($e^{-\beta t}$)
Dilution Factor
Freeloader Return Time
Return Time β^{-1} ($e^{-\beta t}$)
Dilution Factor
e
Eigenvalue Magnitude
|λ|
Dilution Factor
Eigenvalue Angle
θ
Dilution Factor

Supplementary Figure 2: Early warning indicators of ecosystem collapse. A compilation of results from all of the three experiments for: **(a)** Mean Equilibrium Density for each population, **(b)** CV – Coefficient of Variation for each population, **(c)** *AR*(*1*) autocorrelation (see Supplementary Note 5) for each population, which was measured from Day 2 to the last day, **(d)** Return time (see Supplementary Note 5), and **(e)** $|\lambda|$ and θ - magnitude and argument of the eigenvalues. Data was filtered (see Supplementary Note 3) to exclude any obviously dying trajectories from the three experiments. Error bars represent standard errors. The Black data corresponds to experiment from Figs. 1 and 4, Violet to the one from Fig. 2, and Blue to the data from Fig. 3. Error bars represent standard errors and were attained through bootstrapping.

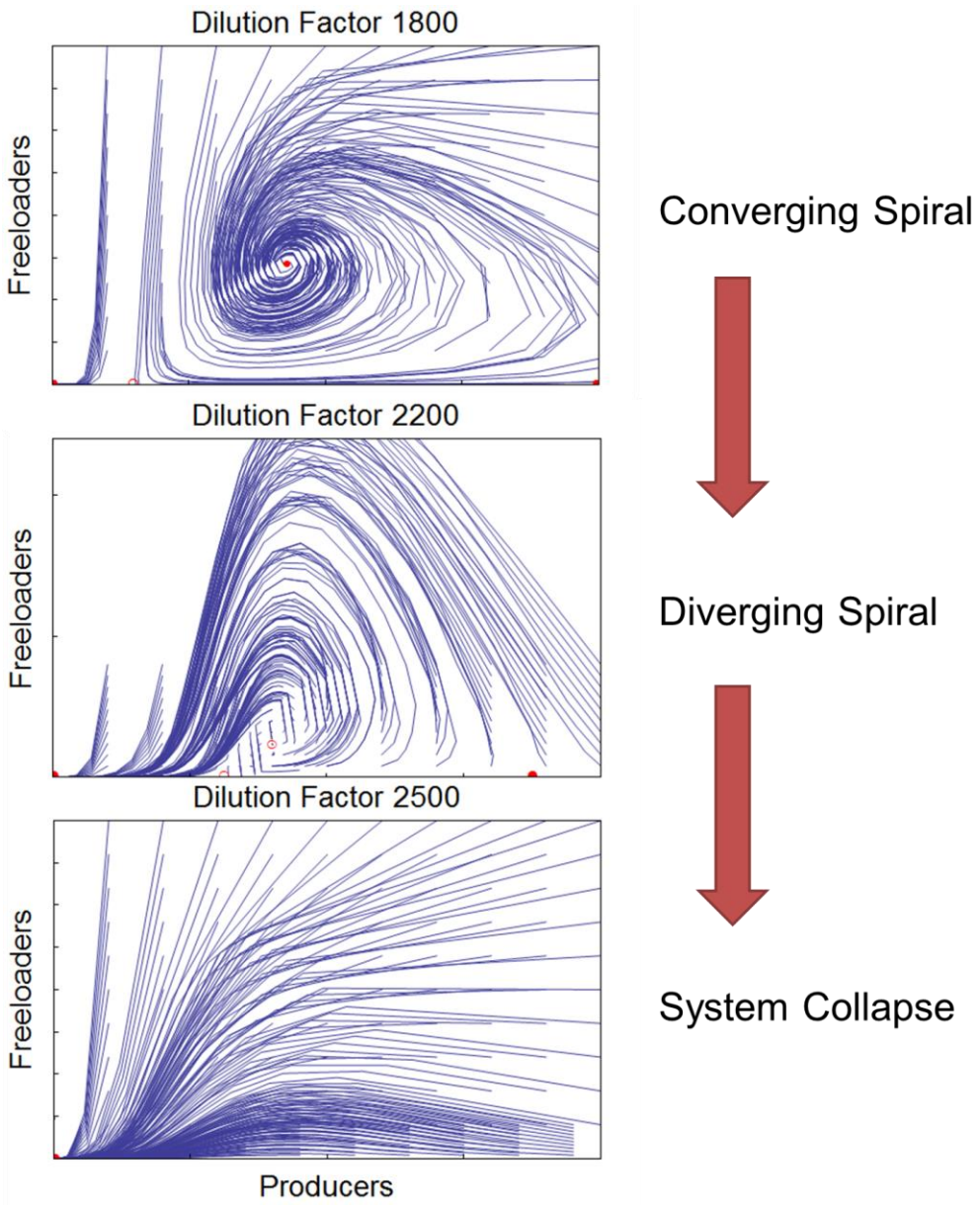

Supplementary Figure 3: Model suggests the systems undergoes a Hopf bifurcation at the critical threshold. A simulation of our model system at 3 DFs near our conjectured critical point (~2100) shows that the trajectories change from a converging spiral to a diverging spiral, indicative of a Hopf bifurcation. Eventually, at high enough Dilution Factors, spiraling behavior is overshadowed by a total population collapse. Fixed points are indicated by solid red dots (stable) or hollow red dots (unstable). The high-producer fixed point on a Dilution Factor of 1800 has been shifted to the left in order to fit on the graph. Direction of motion is counter-clockwise for all dilution factors. All ticks are spaced by an equal yet unnormalized quantity. Simulations were initialized with 100-200 starting points (arranged in a grid), and run for 20-30 iterations.

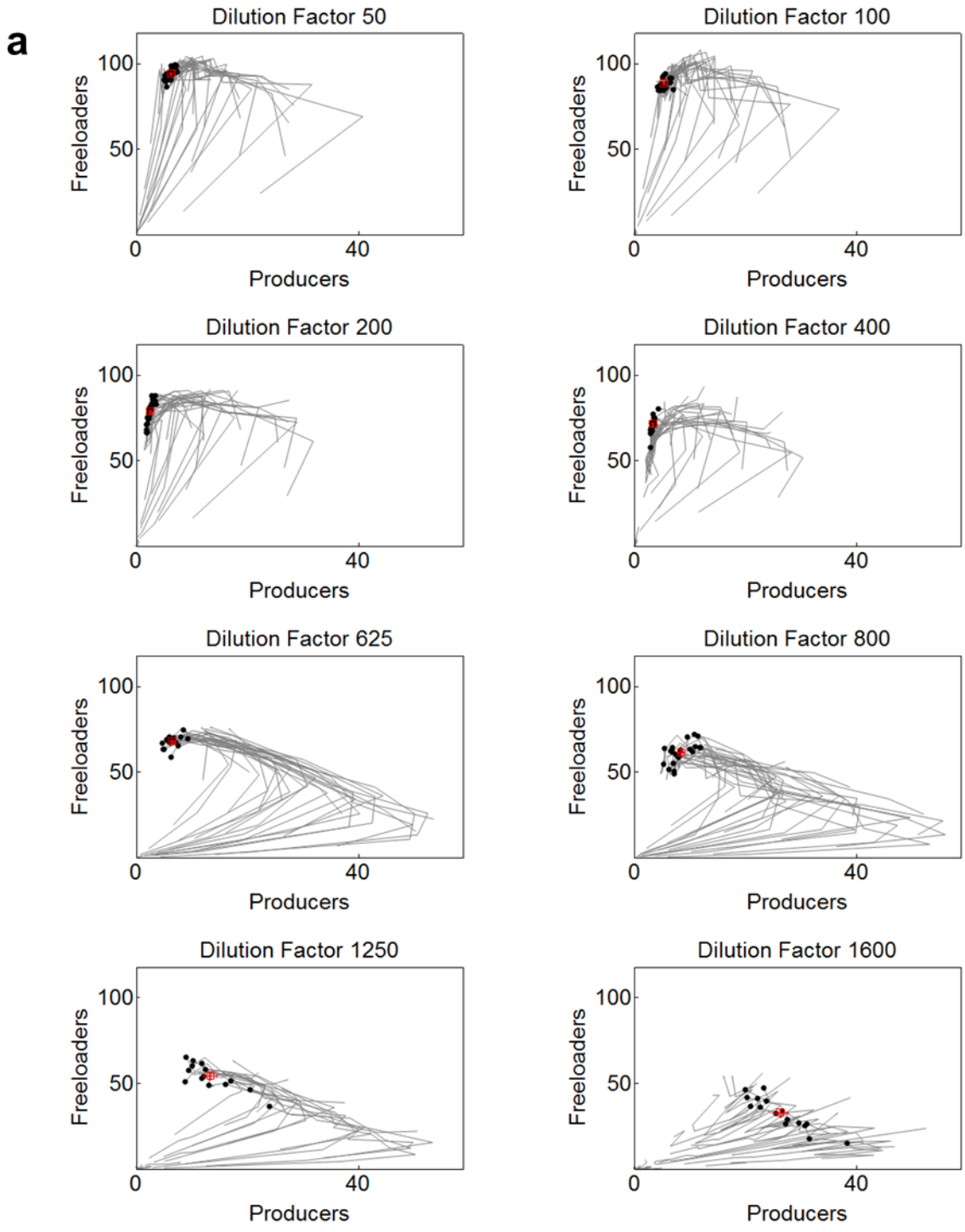
a
Dilution Factor 50
Dilution Factor 100
Dilution Factor 200
Dilution Factor 400
Dilution Factor 625
Dilution Factor 800
Dilution Factor 1250
Dilution Factor 1600
Freeloaders
Producers
0
40
50
100

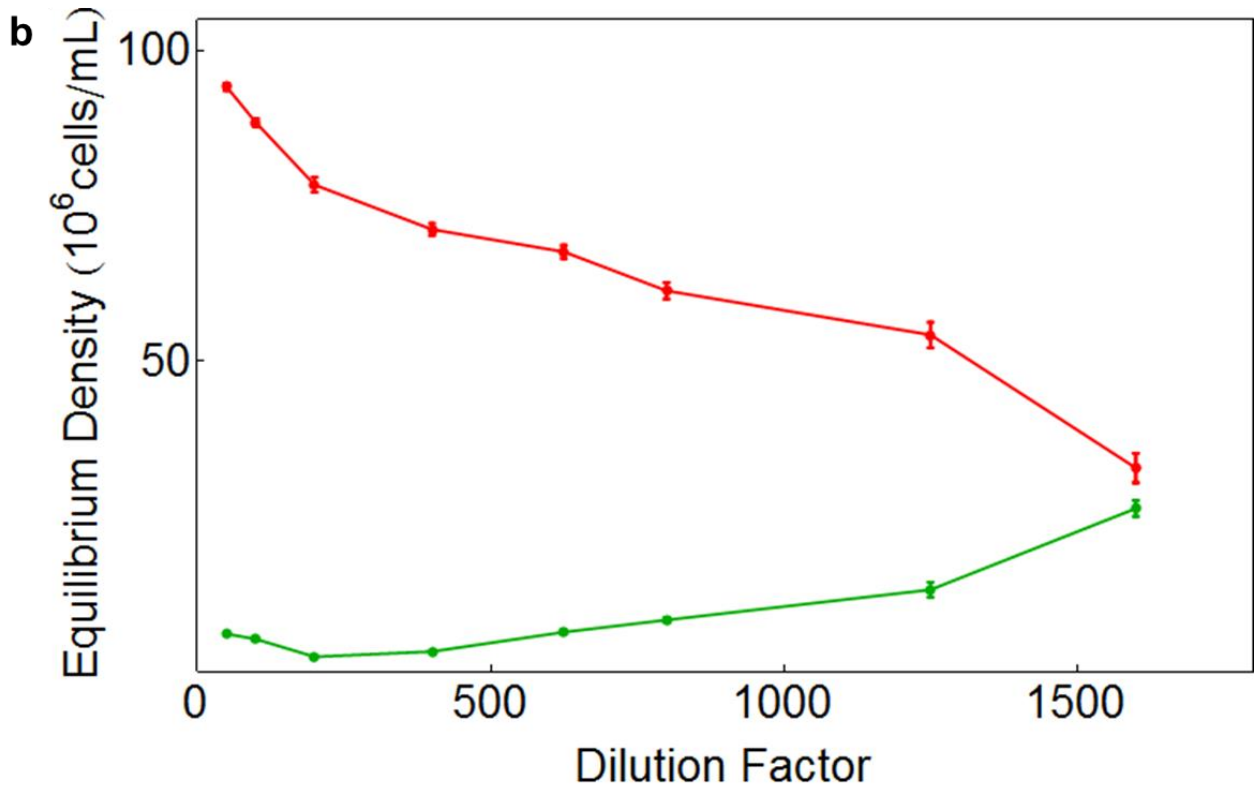

Supplementary Figure 4: Spiraling trajectory graphs, filtering, and calculation of equilibrium points. (a) The spiraling trajectories of all dilution factors of the 7-day experiment represented in Fig. 3, plotted in gray on the same Producer – Freeloader plane. Population densities are all expressed in units of 10^6 cells/mL. Black points denote the final state of those trajectories that survived the filtering algorithm described in Supplementary Note 3, and which are thus considered to be in equilibrium. The red squares represent the mean of these filtered points with accompanying standard errors – which was further used as an estimate of the equilibrium point of the spirals. **(b)** These were plotted as a function of the dilution factor for both the Producers (green) and Freeloaders (red).

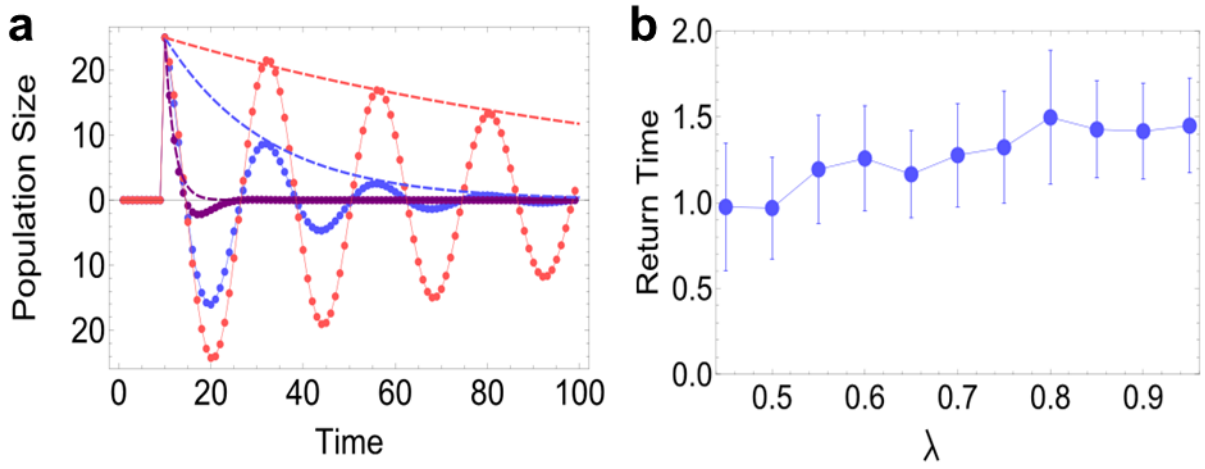

Supplementary Figure 5: Return to equilibrium after a perturbation as a function of the magnitude of the eigenvalue. (a) We show the dynamical response of a population whose dynamics are governed by equation (3) (only one of the populations, x, is plotted), with a Jacobian matrix with imaginary eigenvalues (see equation (21)). The dynamics are characterized by damped oscillatory behavior, and thus they are described by two timescales; (i) the timescale of oscillations and (ii) the decay of the envelope of the oscillations. For simplicity we just plot the deterministic dynamics (noise strength is assumed to be 0). The orange dots correspond to $|\lambda|$=0.99, blue dots correspond to $|\lambda|$=0.95, and purple correspond to $|\lambda|$=0.75. All other parameters ($\theta=15^o$,$Q=45^o$, $r=1$) are kept constant. We find that while the envelope of the fluctuations (dashed lines) decays ever more slowly as $|\lambda|\rightarrow 1$, the short term decay is little sensitive to the value of $|\lambda|$. Both time and Return Time units are Days. **(b)** We repeated this simulation in the presence of noise ($\sigma = 1$). The return time was naively estimated by fitting the short-term decay (over the first eight days) to an exponential decay function (mimicking what an unsuspecting researcher might do with experimental data collected in the field). As expected, we found that this "naïve estimate" of the decay time scales only weakly with $|\lambda|$, since it is the envelope what should decay more and more slowly as $|\lambda|$ increases, while the short term dynamics are mainly governed by the complex argument of the eigenvalue (θ). Error bars represent standard deviation of the list of return times obtained in 50 simulations.

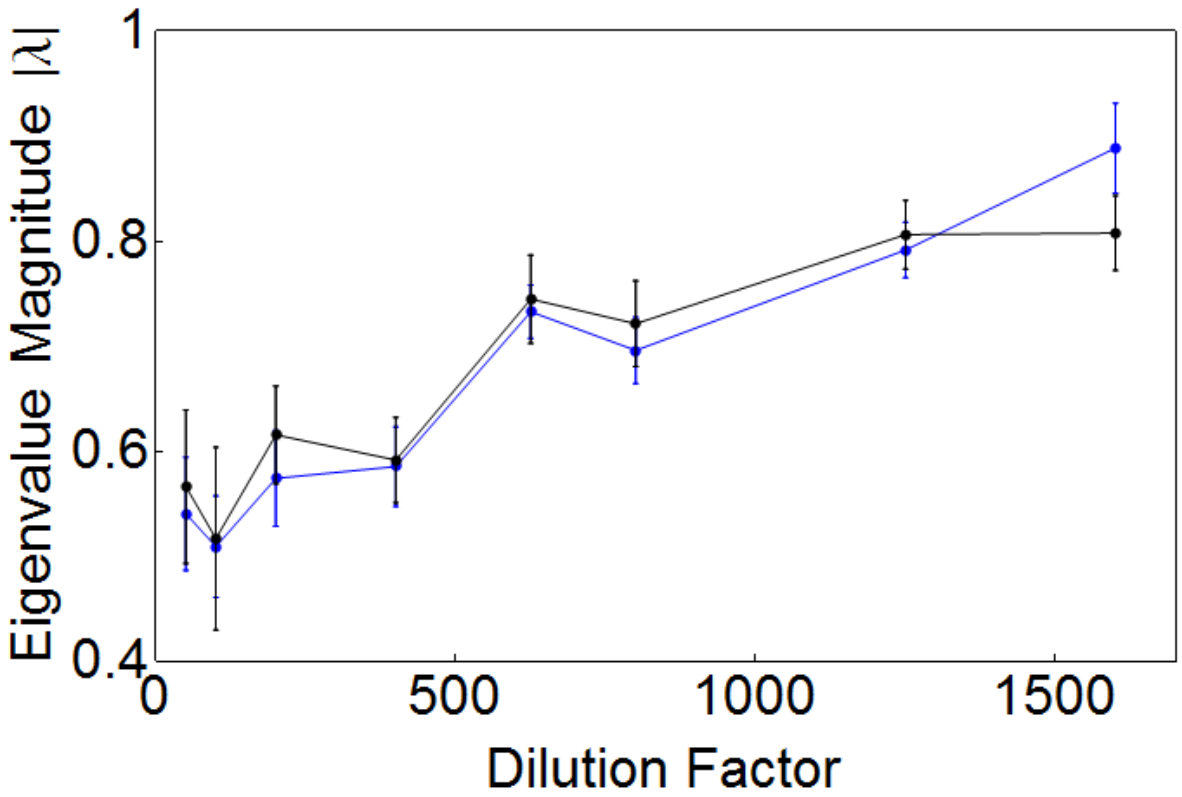

Supplementary Figure 6: Comparison of eigenvalue magnitude results from two different analysis methods. The experiment described in Fig. 3 was analyzed in two different ways: a functional minimization of four parameters given a fixed point (Method 1, blue), and a parameter-fitting algorithm calculated over four parameters as well as the fixed point location (Method 2, black). The differences between these methods are described in Supplementary Note 4. The eigenvalue magnitudes calculated using these methods were plotted against the dilution factor. Error bars represent standard error, and were obtained through bootstrapping the trajectories included in the analysis, as well as the location of the fixed point for Method 1.

Supplementary Tables

Supplementary Table 1: The values used for the dynamical simulation of the producer-freeloader system, as described in Supplementary Note 6.

Parameter	**Value in simulation**
γ_l	0.31 hr^{-1}
γ_h	0.47 hr^{-1}
W	276 μL^{-1}
T_{lag}	3 hr
b	0.06
a	0.075
K	83,341 μL^{-1}

Supplementary Notes

Supplementary Note 1: Analytical derivation of lag-1 autocorrelation (*AR*(1)) in species interactions

In the framework of a first-order multivariate autoregressive model (MAR(1)) model [30,46], we derive the asymptotic behaviors of lag-1autocorrelation and the variance for each population in a two-species ecosystem as the magnitude of the dominant eigenvalue of the interaction matrix approaches 1. We show that for an ecosystem with two interacting species, the *AR*(*1*) for each species is generally not expected to be a good indicator of critical slowing down. When the species interactions lead to oscillatory dynamics (i.e. when the Jacobian has imaginary eigenvalues $\lambda_{1,2}=|\lambda|e^{\pm i\theta}$), the *AR*(*1*) does not approach ~*1* as the magnitude of the eigenvalue ($|\lambda|$) approaches *1*; instead *AR*(*1*) approaches the real part of the eigenvalue. Only when the trajectories do not have an oscillatory component (i.e. when the eigenvalues of the Jacobian, λ_{dom} and λ_2, are real), the *AR*(*1*) approaches ~*1* as the dominant eigenvalue λ_{dom} approaches *1*. In contrast to the *AR*(*1*), we show that the variance for each population is expected to diverge as the dominant eigenvalue approaches 1, regardless of whether the eigenvalues are real or complex.

We note that the results here are only meant to show the qualitative behaviors of these two commonly used statistical indicators based on time series of a single species (partial information) when a two-species ecosystem is very close to a bifurcation associated with critical slowing down. In general, the projection of each population on the dominant eigenvector will also vary in the approach of bifurcations; thus despite their asymptotic behaviors, the indicators based on a single population may not be monotonically increasing before population collapse and this will complicate their usefulness as warning signals. However, if we also have time series of the interacting species (complete information), then we should follow our analysis on the phase plane to fit the Jacobian) and transform the variables by projecting onto the eigenvectors, which gives a more complete measure of stability of the system[5].

MAR(1) model of a two-species ecosystem: Let us assume a two-species ecosystem undergoing discrete dynamics as in our experiments. Let X_t and Y_t represent the population size for both species at day *t*. Let's also define the population size of both species at equilibrium as X^* and Y^*. The coupled population dynamics near equilibrium is given by the discrete equation:

$$\begin{pmatrix} X_{t+1}-X^* \\ Y_{t+1}-Y^* \end{pmatrix} = J\cdot\begin{pmatrix} X_t-X^* \\ Y_t-Y^* \end{pmatrix}+\begin{pmatrix} \xi_{x,t} \\ \xi_{y,t} \end{pmatrix}, \qquad (3)$$

where J represents the Jacobian matrix (also called "interaction matrix"). $\xi_{x,t}$ and $\xi_{y,t}$ are Gaussian while noise (we will drop the subscript *t* for convenience) and represent a random "extrinsic" noise term acting independently on each population. We assume that the extrinsic noise term for the two different populations is uncorrelated:

$$\left\langle \xi_x \xi_y \right\rangle = 0\,, \tag{4}$$

and also that it is not correlated with the population size:

$$\left\langle \xi_x X_t \right\rangle = \left\langle \xi_x Y_t \right\rangle = \left\langle \xi_y X_t \right\rangle = \left\langle \xi_y Y_t \right\rangle = 0\,. \tag{5}$$

Furthermore, to simplify our equations we introduce the following notation:

$$\left\langle \xi_x^{\,2} \right\rangle = \sigma^2\,,\ x_t = X_t - X^*,\ y_t = Y_t - Y^*, \tag{6}$$

where σ^2 denotes the strength of the intrinsic noise term, and x_t and y_t represent the deviation from equilibrium for both species.

Using this notation, equation (3) can be rewritten as:

$$\begin{pmatrix} x_{t+1} \\ y_{t+1} \end{pmatrix} = J \cdot \begin{pmatrix} x_t \\ y_t \end{pmatrix} + \begin{pmatrix} \xi_x \\ \xi_y \end{pmatrix}, \tag{7}$$

or, in vector form:

$$\vec{\boldsymbol{x}}_{t+1} = J \cdot \vec{\boldsymbol{x}}_t + \vec{\boldsymbol{\xi}}\,. \tag{8}$$

In order to compute the covariance matrix, we first take the transpose of this equation:

$$\vec{\boldsymbol{x}}_{t+1}^{\boldsymbol{T}} = \vec{\boldsymbol{x}}_t^{\boldsymbol{T}} \cdot J^{\boldsymbol{T}} + \vec{\boldsymbol{\xi}}^{\boldsymbol{T}}\,. \tag{9}$$

Then we calculate the dot product of Equations (8) and (9).

$$\vec{\boldsymbol{x}}_{t+1} \cdot \vec{\boldsymbol{x}}_{t+1}^{\boldsymbol{T}} = \left(J \cdot \vec{\boldsymbol{x}}_t + \vec{\boldsymbol{\xi}} \right)\left(\vec{\boldsymbol{x}}_t^{\boldsymbol{T}} \cdot J^{\boldsymbol{T}} + \vec{\boldsymbol{\xi}}^{\boldsymbol{T}} \right) = J \cdot \vec{\boldsymbol{x}}_t \cdot \vec{\boldsymbol{x}}_t^{\boldsymbol{T}} \cdot J^{\boldsymbol{T}} + J \cdot \vec{\boldsymbol{x}}_t \cdot \vec{\boldsymbol{\xi}}^{\boldsymbol{T}} + \vec{\boldsymbol{\xi}} \cdot \vec{\boldsymbol{x}}_t^{\boldsymbol{T}} \cdot J^{\boldsymbol{T}} + \vec{\boldsymbol{\xi}} \cdot \vec{\boldsymbol{\xi}}^{\boldsymbol{T}}\,. \tag{10}$$

In order to compute the covariance matrix, we take the time average (or, if the system is ergodic, the average over an ensemble of replicate populations at a given time) at both sides of this equation:

$$\left\langle \vec{\boldsymbol{x}}_{t+1} \cdot \vec{\boldsymbol{x}}_{t+1}^{\boldsymbol{T}} \right\rangle = \left\langle J \cdot \vec{\boldsymbol{x}}_t \cdot \vec{\boldsymbol{x}}_t^{\boldsymbol{T}} \cdot J^{\boldsymbol{T}} \right\rangle + \left\langle J \cdot \vec{\boldsymbol{x}}_t \cdot \vec{\boldsymbol{\xi}}^{\boldsymbol{T}} \right\rangle + \left\langle \vec{\boldsymbol{\xi}} \cdot \vec{\boldsymbol{x}}_t^{\boldsymbol{T}} \cdot J^{\boldsymbol{T}} \right\rangle + \left\langle \vec{\boldsymbol{\xi}} \cdot \vec{\boldsymbol{\xi}}^{\boldsymbol{T}} \right\rangle. \tag{11}$$

Since the system is in equilibrium, we find that:

$$\left\langle \vec{\boldsymbol{x}}_{t+1} \cdot \vec{\boldsymbol{x}}_{t+1}^{\boldsymbol{T}} \right\rangle = \left\langle \vec{\boldsymbol{x}}_t \cdot \vec{\boldsymbol{x}}_t^{\boldsymbol{T}} \right\rangle = \begin{pmatrix} \left\langle x_t^2 \right\rangle & \left\langle x_t y_t \right\rangle \\ \left\langle x_t y_t \right\rangle & \left\langle y_t^2 \right\rangle \end{pmatrix} = C\,, \tag{12}$$

where *C* stands for the covariance matrix. In addition, since the noise term $\vec{\boldsymbol{\xi}}$ is assumed to be uncorrelated with the population size deviation $\vec{\boldsymbol{x}}_t$ we also find that:

$$\left\langle J \cdot \vec{\boldsymbol{x}}_t \cdot \vec{\boldsymbol{\xi}}^{\boldsymbol{T}} \right\rangle = \left\langle \vec{\boldsymbol{\xi}} \cdot \vec{\boldsymbol{x}}_t^{\boldsymbol{T}} \cdot J^{\boldsymbol{T}} \right\rangle = 0. \tag{13}$$

and by assumption $\left\langle \xi_x \xi_y \right\rangle = 0$ and:

$$\left\langle \xi_x^2 \right\rangle = \left\langle \xi_y^2 \right\rangle = \sigma^2 . \tag{14}$$

For simplicity we assumed that $\sigma^2 = \sigma_x^2 = \sigma_y^2$. In general the magnitude of extrinsic noise is different for two species, but this does not change the results on asymptotic behaviors. We find:

$$\left\langle \vec{\boldsymbol{\xi}} \cdot \vec{\boldsymbol{\xi}}^{\boldsymbol{T}} \right\rangle = \sigma^2 \begin{pmatrix} 1 & 0 \\ 0 & 1 \end{pmatrix} = \sigma^2 I . \tag{15}$$

where *I* stands for the identity matrix. Therefore, Equation (11) takes the form:

$$\left\langle \vec{\boldsymbol{x}}_t \cdot \vec{\boldsymbol{x}}_t^{\boldsymbol{T}} \right\rangle = J \cdot \left\langle \vec{\boldsymbol{x}}_t \cdot \vec{\boldsymbol{x}}_t^{\boldsymbol{T}} \right\rangle \cdot J^{\boldsymbol{T}} + \left\langle \vec{\boldsymbol{\xi}} \cdot \vec{\boldsymbol{\xi}}^{\boldsymbol{T}} \right\rangle \tag{16}$$

or:

$$C = J \cdot C \cdot J^{\boldsymbol{T}} + \sigma^2 I . \tag{17}$$

In order to compute the *AR*(1), we follow essentially the same approach: We multiply both sides of equation (7) by the transpose vector $\vec{\boldsymbol{x}}_t^{\boldsymbol{T}}$. Then, just as we did above, we take time averages at both sides of the equation. By doing this we find the following relationship between the lag-1 correlation matrix and the covariance matrix and the Jacobian:

$$B = \begin{pmatrix} \left\langle x_{t+1} x_t \right\rangle & \left\langle x_{t+1} y_t \right\rangle \\ \left\langle y_{t+1} x_t \right\rangle & \left\langle y_{t+1} y_t \right\rangle \end{pmatrix} = J \cdot C . \tag{18}$$

The *AR*(1) for the two populations can be calculated from this matrix, since they are defined as:

$$AR(1)_x = \frac{\left\langle x_{t+1} x_t \right\rangle}{\left\langle x_t^2 \right\rangle}, \tag{19}$$

$$AR(1)_y = \frac{\left\langle y_{t+1} y_t \right\rangle}{\left\langle y_t^2 \right\rangle}. \tag{20}$$

The variances of both populations for Jacobians with complex eigenvalues: We have reached an equation that describes the covariance matrix as a function of the Jacobian and the extrinsic noise strength σ^2. In order to find the final closed form analytical equation for the covariances and variances from each species, as well as the *AR*(1), we need to know the Jacobian matrix. We first study the case where both eigenvalues are complex conjugate of each other. The Jacobian can be decomposed in its eigenvectors (assuming that the matrix is not defective):

$$J = P\begin{pmatrix} |\lambda| e^{i\theta} & 0 \\ 0 & |\lambda| e^{-i\theta} \end{pmatrix} P^{-1}, \tag{21}$$

where *P* is the matrix whose columns are the eigenvectors of *J*. Since by assumption the Jacobian has complex eigenvalues, its two eigenvectors are complex conjugate of each other:

$$P = \begin{pmatrix} |u_1| e^{i\varphi_1} & |u_1| e^{-i\varphi_1} \\ |u_2| e^{i\varphi_2} & |u_2| e^{-i\varphi_2} \end{pmatrix}. \tag{22}$$

Therefore, the Jacobian can be written in terms of the magnitude and complex argument of its eigenvalues ($|\lambda|$ and θ), as well as the two parameters that characterize its eigenvectors, (r and Q, where $Q = \varphi_2 - \varphi_1$, and $r = |u_2|/|u_1|$.). By inserting equation (22) into equation (21), we get:

$$J = \begin{pmatrix} J_{11} & J_{12} \\ J_{21} & J_{22} \end{pmatrix} = |\lambda| \begin{pmatrix} Cos[\theta] + Cot[Q] Sin[\theta] & -r^{-1} Csc[Q] Sin[\theta] \\ r\ Csc[Q] Sin[\theta] & Cos[\theta] - Cot[Q] Sin[\theta] \end{pmatrix}. \tag{23}$$

Finally, we can insert equation (23) into equation (17), and solve to obtain analytical expressions for the variances of both populations as well as their covariance. The expressions are lengthy and not particularly informative. However, we are only interested in their behavior as the absolute magnitude of the eigenvalue approaches 1, a situation corresponding to critical slowing down. We find that in the limit when $|\lambda| \rightarrow 1$:

$$\left\langle x_t^2 \right\rangle \sim \frac{\sigma^2}{1-|\lambda|} \left(\frac{Csc[Q]}{2} \right)^2 \left(\frac{1+r^2}{r^2} \right), \tag{24}$$

$$\left\langle y_t^2 \right\rangle \sim \frac{\sigma^2}{1-|\lambda|} \left(\frac{Csc[Q]}{2} \right)^2 \left(\frac{1+r^2}{r^2} \right), \tag{25}$$

$$\left\langle x_t y_t \right\rangle \sim \frac{\sigma^2}{1-|\lambda|} \left(\frac{Csc[Q]}{2} \frac{Cot[Q]}{2} \right) \left(\frac{1+r^2}{r} \right). \tag{26}$$

Therefore, the variance for both populations diverges as $|\lambda| \rightarrow 1$.

AR(1) for Jacobian matrices with complex eigenvalues: We can compute the *AR*(1) by inserting equation (23) into equation (18). We find:

$$AR(1)_x = \frac{\langle x_{t+1}x_t \rangle}{\langle x_t^2 \rangle} = \frac{J_{11}\langle x_t^2 \rangle + J_{12}\langle x_t y_t \rangle}{\langle x_t^2 \rangle} = J_{11} + J_{12}\frac{\langle x_t y_t \rangle}{\langle x_t^2 \rangle}. \quad (27)$$

$$AR(1)_y = \frac{\langle y_{t+1}y_t \rangle}{\langle y_t^2 \rangle} = \frac{J_{21}\langle y_t^2 \rangle + J_{22}\langle x_t y_t \rangle}{\langle y_t^2 \rangle} = J_{21} + J_{22}\frac{\langle x_t y_t \rangle}{\langle y_t^2 \rangle}. \quad (28)$$

Now we can insert equations (23-26) into equations (27-28), and express the *AR*(1) as a function of the eigenvalues and the parameters characterizing the eigenvectors ($|\lambda|$, θ, r, Q). As it was the case for the variances, the analytical equations calculated this way are long and not particularly informative. However, we can take the limit where $|\lambda| \rightarrow 1$ and find out what the behavior of the *AR*(1) in the vicinity of the critical transition should be. What we find is that the *AR*(1) does not approach 1, as it does for single-species ecosystems. Instead, the *AR*(1) behaves as:

$$AR(1)_x = AR(1)_y \sim |\lambda| Cos[\theta]. \quad (29)$$

Therefore, for two-species ecosystem with strong interactions that lead to oscillatory behavior (typical of many consumer-resource ecosystems, such as predator-prey, host-parasitoid, or host-parasite) and characterized by complex eigenvalues, we conclude that the *AR*(1) for each population is not generally expected to approach 1 as the ecosystem approaches a critical transition characterized by $|\lambda| \rightarrow 1$ (i.e. critical slowing down). Thus, the failure of AR(1) in our experimental observation may be due to the fact that: 1) while the magnitude of the eigenvalue increases, the real part of the eigenvalue does not necessarily increase monotonically; 2) the relatively small sample size of our experiment tends to underestimate AR(1), based on simulations results in MAR(1) model. Meanwhile, the variance of each population is still expected to diverge as shown in equations (24-25). Together with the experimental observations (Fig. 4 and Supplementary Fig. 2b), our results suggest that variation of a single population may be a more reliable indicator than lag-1 autocorrelation.

Variance and AR(1) for Jacobian matrices with real eigenvalues: We can use the same procedure to show that, for Jacobian matrices with real eigenvalues, the *AR*(1) does indeed approach 1 as the dominant eigenvalue approaches 1. In addition, the variance also diverges, as it did for the case of complex eigenvalues. In order to do this, we first write down a general Jacobian matrix with real eigenvalues (we will denote the dominant eigenvalue as λ_{dom}, and the other one as λ_2). The eigendecomposition of the Jacobian on the basis of its eigenvectors is:

$$J = P\begin{pmatrix} \lambda_{dom} & 0 \\ 0 & \lambda_2 \end{pmatrix}P^{-1}. \quad (30)$$

For convenience, we use eigenvectors of length 1. This allows us to write down the matrix P as:

$$P = \begin{pmatrix} Cos[\alpha] & Cos[\beta] \\ Sin[\alpha] & Sin[\beta] \end{pmatrix}, \tag{31}$$

where α and β and are the angles formed by each eigenvector with the x axis in the phase space formed by the two populations. Combining equations (30) and (31), we find the following parameterization of J as a function of its two eigenvalues (λ_{dom} and λ_2), and the two angles that characterize its eigenvectors (α and β):

$$J = Csc[\alpha-\beta]\begin{pmatrix} \lambda_2 Cos[\beta]Sin[\alpha] - \lambda_{dom} Cos[\alpha]Sin[\beta] & (\lambda_{dom}-\lambda_2)Cos[\alpha]Cos[\beta] \\ -(\lambda_{dom}-\lambda_2)Sin[\alpha]Sin[\beta] & \lambda_{dom} Cos[\beta]Sin[\alpha] - \lambda_2 Cos[\alpha]Sin[\beta] \end{pmatrix}. \tag{32}$$

In order to compute the *AR*(1), all we have to do is to insert equation (32) into equation (17) and find all the elements in the covariance matrix. As before, we are only interested in the behavior of these equations as λ_{dom} approaches 1. In this limit, we find:

$$\left\langle x_t^2 \right\rangle \sim \frac{\sigma^2}{1-\lambda_{dom}} \left(\frac{Csc[\alpha-\beta]}{\sqrt{2}} \right)^2 Cos^2[\alpha], \tag{33}$$

$$\left\langle y_t^2 \right\rangle \sim \frac{\sigma^2}{1-\lambda_{dom}} \left(\frac{Csc[\alpha-\beta]}{\sqrt{2}} \right)^2 Sin^2[\alpha], \tag{34}$$

$$\left\langle x_t y_t \right\rangle \sim \frac{\sigma^2}{1-\lambda_{dom}} \left(\frac{Csc[\alpha-\beta]}{2} \right)^2 Sin[2\alpha]. \tag{35}$$

Equations (33) and (34) show that the variances of both populations diverge as $\lambda_{dom} \to 1$. We can use these equations, together with equations (27-28) to find the *AR*(1). In the same limit, when $\lambda_{dom} \to 1$, the *AR*(1) for both individual populations approaches 1. One situation that arises when dealing with real eigenvalues is that if the projection of a species on the dominant eigenvector is very small (i.e., if $Cos[\alpha] << 1$), the variance may not diverge noticeably until the dominant eigenvalue is extremely close to 1. In conclusion, we have shown that when the eigenvalues are both real both the variance and the *AR*(1) are expected to be good indirect indicators of critical slowing down.

Supplementary Note 2: Discussion of the Return Time

In the presence of strong inter-species interactions that lead to an oscillatory component, the dynamics of both involved species will be affected by those oscillations. In the main text we argue that the return time may be hard to estimate in these situations. Indeed, in Supplementary Fig. 5 we followed what we believe would be the zero-order approach for an experimentalist trying to estimate the return time of a single species; this is, recording population size as a function of time following a perturbation or disturbance, and then fitting the observed relaxation to equilibrium to a decaying exponential to find the characteristic time of recovery. This approach has been successfully employed in previous laboratory experiments with a single species [26,27]. Furthermore, one of those experiments [26], was performed on a single-species population consisting of the same producer yeast strain we use here. Therefore, it is natural to replicate the experimental procedures that we have already established successfully for the pure freeloader population, to estimate the return time in the presence of the freeloader strain. As shown in Supplementary Fig. 2d, we did not observe a strong increase in the return time as a function of the dilution factor. Only for the producer population we did find an increase in the return time at DF=2000, although the data is very noisy at that high DF, and we also observe a decline in the return time for the freeloader population. Therefore, it appears as if the return time is not a reliable indicator of critical slowing down in our population.

In order to explain this, we resort to theory and simulations. We use a generic Jacobian matrix with complex eigenvalues to determine the population dynamics of a two-species ecosystem in following a perturbation (which we apply to a population that was previously on equilibrium by artificially increasing the size of one of the populations). In Supplementary Fig. 5a we plot the response of a population to a perturbation for three different values of $|\lambda|$ (0.75, 0.95 and 0.99). We find that the dynamics of both populations are characterized by damped oscillations, as expected. As $|\lambda|$ increases, we notice that the envelope of the oscillations does indeed decay more slowly. However, the short-term dynamics (which would correspond to the naïve estimate of the return time that we applied to our experiments) is little affected by $|\lambda|$. We confirmed that this is still the case in the presence of noise (Supplementary Fig. 5b), where we estimated the return time for a set of different values of $|\lambda|$ using the naïve approach.

This analysis indicates that in order to estimate the component of the return time that does increase as $|\lambda| \rightarrow 1$, we would need to observe several cycles in order to be able to estimate the decay of the envelope of the oscillations. The total number of cycles that need to be observed depend only on the argument of the complex eigenvalues θ. This might lead to the requirement of very long time traces, a hurdle that cannot be overcome by increasing the sample size and observing for a shorter time. In our experiments, the envelope decay could not be seen with enough resolution for us to be able to estimate the return time.

Supplementary Note 3: Filtering of Raw Data

At higher dilution factors, some trajectories become unstable and tend towards extinction. Trajectories whose final-day population was less than 5×10^5 producers per mL were excluded from our analysis of fixed points and statistical indicators, as only populations that survived were relevant. For the data from the 9-day experiment (shown in Figs. 1, 4), two trajectories at a dilution factor (DF) of 2000 were also excluded because they were clearly heading towards extinction (even though the producers had not explicitly dropped below 5×10^5cells/mL).

For the experiments represented in Figs. 2 and 3, populations started at different initial conditions; an additional filtering algorithm was utilized to select populations that had approached equilibrium. Trajectories whose logarithmic population densities changed less than 10% (for the experiment from Fig. 2) or 25% a day (for the experiment from Fig. 3) were defined to be in equilibrium. The mean of these populations around equilibrium on the final 3 days of the 14-day experiment or the last day of the 7-day experiment was used as an estimate of the fixed point (see Supplementary Fig. 4). Due to the filter, this amounted to typically n=20 points being averaged. These estimates of the fixed points were later used to fit the Jacobian matrix (Method 1) as explained in Note S4. However, the actual trajectories analyzed for the eigenvalues were filtered by the 5×10^5 producers/mL criterion for survival, and the first day was dropped due to the apparent non-linear behavior far from the fixed point. Furthermore, for the calculation of lag-1 autocorrelation, only data points that had logarithmic producer and freeloader densities within 25% of the estimated fixed point were used. The specific data used in each main-text figure is described in Supplementary Note 7.

Supplementary Note 4: Eigenvalue Computational Methods

Method 1: The first method, is a least-squares functional minimization across the 4 parameters of J, given a known equilibrium point (X^*, Y^*). This point is estimated for each dilution factor by the mean of the filtered data of the trajectories as shown in Supplementary Fig. 4. The filter algorithm (described above) selects for data points from the last two days whose logarithmic population densities both changed by less than 25% a day.

Next, an error function ε is built based on the squared difference between the true value of a trajectory's motion and its estimation given an arbitrary Jacobian matrix J**:**

$$\varepsilon = \sum_t \left[\begin{pmatrix} X_{t+1} - X^* \\ Y_{t+1} - Y^* \end{pmatrix} - J \cdot \begin{pmatrix} X_t - X^* \\ Y_t - Y^* \end{pmatrix} \right]^2 \qquad (36)$$

This sum is expanded by inputting the trajectory data (X_t, Y_t) from each day and each replicate, as well as substituting in the equilibrium point (X^*, Y^*) found previously. Then, this error function of four variables is numerically minimized to locate the best estimate for J. This method is essentially the least-squares estimation in linear regression.

Method 2: A second method was also used. First, a set of possible J matrices was constructed from varying ranges of six parameters: the real and imaginary parts of the eigenvalues and the eigenvectors, as well as the location of the fixed point (X^*, Y^*). The matrix eigendecomposition J of a given set of parameters is then used to find an error value for that set of parameters. By summing the individual errors from within each replicate and day, the total error ε is calculated from equation (36). The set of parameters that has the smallest total error value is deemed the best fit. Typically, around 10 values are tried for each parameter – so there are a total of a million combinations of six parameters – and this can be iterated for increased precision.

In Fig. 3, the results displayed come from Method 1 analysis. Both analysis methods yielded very similar results (Fig. S6). There are tradeoffs in using each analysis: Method 2 does not require knowledge of the equilibrium point, but it is much more computationally intensive. Note that in Method 2, it is assumed mathematically that the eigenvalues and eigenvectors are complex, whereas Method 1 leaves open the possibility of purely real results. The fixed point (X^*, Y^*) is assumed to be real and non-negative. To attain error estimates of these parameters, the analysis was bootstrapped through a random selection of the trajectory data points and fixed point. This fixed point is randomized via a bivariate normal distribution around the estimated fixed point (see Supplementary Note 3), with a standard deviation equal to the estimation's standard error (Supplementary Fig. 4).

While utilizing Method 1, we sometimes come across trajectories that give real pairs of eigenvalues, instead of complex conjugates. This generally either occurs at the lowest dilution factors (where the dynamics are too quick to be able to differentiate between real and complex eigenvalues) or at the highest dilution factors (where noise may drown out some properties of the signal). This also may be a consequence of our linearizing the dynamics of the trajectories. For the data shown in Fig. 3, only the largest dilution factor (DF 1600) had a significant number of real-eigenvalue trajectories. Thus, the mean eigenvalue magnitude was calculated by averaging the complex magnitude (in the cases of complex eigenvalues) or the dominant eigenvalue (in the cases of real eigenvalues), giving $|\lambda| = 0.88 \pm 0.04$. For comparison, when we constrained the analysis to force the eigenvalues into being complex, we found that $|\lambda| = 0.80 \pm 0.03$. In general, the difference between the dominant real eigenvalue and the complex magnitude is small when analyzed for the same trajectories. Furthermore, because constraining the eigenvalues to be complex can lead to a quantitatively worse fit, we think it is justified to analyze the eigenvalues in this mixed fashion.

Supplementary Note 5: Calculation of lag-1 Autocorrelation and Return Time

For each population, lag-1autocorrelation (also referred to as *AR*(*1*)) is defined as:

$$AR(1)_x = \frac{\left\langle \left(X_{t+1} - X^*\right)\left(X_t - X^*\right)\right\rangle}{\left\langle \left(X_t - X^*\right)^2\right\rangle} = \frac{\sum_s \sum_{t=1}^{T-1} \left(x_{t+1}^s - \bar{x}_{t+1}\right)\left(x_t^s - \bar{x}_t\right)}{\sum_s \sum_{t=1}^{T-1} \left(x_t^s - \bar{x}_t\right)^2} \qquad (37)$$

where x_t^s is the population density of replicate trajectory *s* on day *t*, $\bar{x}_t$ is the mean density of all replicates on day *t*, and *T* is the total number of days in the experiment. To estimate this from our data, we first collated the trajectories (*s*) whose producer and freeloader densities were logarithmically within 25% of the mean final population size (See Supplementary Note 3). From this filtered data from each day *t* of the experiment, we then calculated the mean population size across all the trajectories from each day ($\bar{x}_t$). Then, we evaluated the expected values using equation (37), applied to every two-day interval (x_t, x_{t+1}) from every replicate *s* of the experiment, from the first day (*t*=1) to the penultimate day (*t*=*T*-1). This calculation is independently performed for both the producer and freeloader populations. Errors were calculated by bootstrapping both the trajectories and the two-day intervals.

Return times were calculated by fitting an exponential to the time series of each population. Only data past the first inflexion point on each graph was used, to account for the initial overshoot (this is caused by the oscillatory behavior of the coupled producer-freeloader dynamics [35].). The return time is the inverse of the exponential parameter *c* in $a + b\, e^{ct}$, (where *t* represents the time in the discrete dynamics) and is averaged across the replicate trajectories of each dilution factor. Errors were determined by taking the standard error of the return times of each individual trajectory. Further discussions on the estimation of the return time in oscillatory dynamics are found in Supplementary Note 2. Note that these two statistical indicators are calculated based on an ensemble of replicate populations close to equilibrium. Assuming the system is ergodic, the above indicators are equivalent to those calculated from the fluctuations of a single population near equilibrium.

Supplementary Note 6: Simulation of the experimental producer-freeloader ecosystem

We simulated a phenomenological model for our producer-freeloader ecosystem, similar to the one we previously used for this system [26,35,54] . The main assumption of this model is that the growth rate of both producers and freeloaders is density dependent, and given by the equation

$$\begin{pmatrix} \dot{X} \\ \dot{Y} \end{pmatrix} = \left(1 - \frac{X+Y}{K}\right) \begin{pmatrix} r_l \frac{W^n}{W^n + X^n} + r_h \frac{X^n}{W^n + X^n} & 0 \\ 0 & \gamma_l \frac{W^n}{W^n + X^n} + \gamma_h \frac{X^n}{W^n + X^n} \end{pmatrix} \begin{pmatrix} X \\ Y \end{pmatrix} \quad (38)$$

where K is the combined carrying capacity of the system, and W represents a threshold density of producers below which both the producers and the freeloaders grow slowly (at rates γ_l and $r_l = (1-a)\,\gamma_l$, respectively), and above which both grow fast (at rates γ_h and $r_h = (1+b)\,\gamma_h$ respectively). Therefore, this differential equation captures both logistic growth at high producer densities, and the Allee effect from the cooperative behavior of sucrose breakdown at low producer densities.

Notice that the differential equation is not linear, and cannot be solved analytically. After solving it numerically, we evaluated it in incremental time steps of T=23.5 hours (taking into account a 3 hour growth time-lag), and then the producer and freeloader populations are divided by the dilution factor (mimicking the experimental dilution step).

The model is able to capture the increase in the size of the producer population as the environment deteriorated, providing further support to the idea that population sizes are not necessarily a reliable indicator of population health (Supplementary Fig. 1). In our system the producer population size may increase before population collapse because the decrease in freeloader population size is faster, thus reducing competition for resources. The parameters in the model are the same that we used previously [26,35] and are summarized in Supplementary Table 1.

Supplementary Note 7: Elaboration of data analysis procedures for main-text figures

Figure 1: The data from Dilution Factors (DF) 333-2000 came from a 9-day experiment with 6 different dilution factors and about 20 replicates for each. The mean was calculated only using the population sizes from the last day (Day 9). No filtering was done except to remove obviously dying populations (see Supplementary Note 3), which only removed two data points from DF=2000. In a separate experiment, we determined that all trajectories go extinct when DF is 2200 or higher.

Figure 2: This data came from 30 replicates of the same dilution factor (DF=1333) of a 14-day experiment. No trajectories were omitted from any of the graphs. The eigenvalue calculation came from Method 1 (see Supplementary Note 4), which used a fixed point determined from averaging the data present from the last 3 days of the experiment that were selected by the 10% trajectory velocity filtering algorithm described above.

Figure 3: The data points come from a 7-day experiment with 8 different dilution factors with 30 replicates each. Data was filtered by eliminating obviously dying trajectories. Some initial data points were omitted in the analysis due to apparent non-linear behavior of the first-day trajectories. The eigenvalues were obtained by Method 1. The fixed points used to analyze the data came from the estimates from Supplementary Fig. 4b (originating from the velocity filtering algorithm applied to this 7-day experiment).

Figure 4: Data came from the same nine-day experiment as Fig. 1. The coefficient of variability (CV) was calculated as Standard Deviation divided over the Mean from the last day (Day 9) of the experiment. No filtering was done except to remove the two obviously dying replicates from DF=2000.

Supplementary References

1. Sanchez, A. & Gore, J. feedback between population and evolutionary dynamics determines the fate of social microbial populations. *PLoS Biol.* **11,** e1001547 (2013).
2. Celiker, H. & Gore, J. Competition between species can stabilize public-goods cooperation within a species. *Mol. Syst. Biol.* **8,** 621 (2012).
3. Dai, L., Vorselen, D., Korolev, K. S. & Gore, J. Generic indicators for loss of resilience before a tipping point leading to population collapse. *Science* **336,** 1175–1177 (2012).
4. Ives, A. R. Measuring Resilience in Stochastic Systems. *Ecological Monographs* **65,** 217–233 (1995).
5. Ives, A. R., Dennis, B., Cottingham, K. L. & Carpenter, S. R. Estimating community stability and ecological interactions from time-series data. *Ecological Monographs* **73,** 301–330 (2003).
6. Veraart, A. J. *et al.* Recovery rates reflect distance to a tipping point in a living system. *Nature* **481,** 357–359 (2012).